Analytical Modeling of CO_2 Migration in Saline Aquifers for Geological CO_2 Storage

by

Christopher William MacMinn

Submitted to the Department of Mechanical Engineering
in partial fulfillment of the requirements for the degree of

Master of Science in Mechanical Engineering

at the

MASSACHUSETTS INSTITUTE OF TECHNOLOGY

September 2008

Author .....
Department of Mechanical Engineering
August 31, 2008

Certified by .....
Ruben Juanes
Assistant Professor, Civil and Environmental Engineering
Thesis Supervisor

Certified by .....
Anette E. Hosoi
Associate Professor, Mechanical Engineering
Thesis Reader

Accepted by .....
Lallit Anand
Chairman, Department Committee on Graduate Students

Analytical Modeling of CO_2 Migration in Saline Aquifers for Geological CO_2 Storage

by

Christopher William MacMinn

Submitted to the Department of Mechanical Engineering
on August 31, 2008, in partial fulfillment of the
requirements for the degree of
Master of Science in Mechanical Engineering

Abstract

Injection of carbon dioxide into geological formations for long-term storage is widely regarded as a promising tool for reducing global atmospheric CO_2 emissions. Given the environmental and health risks associated with leakage of CO_2 from such a storage site, it is critical to ensure that injected CO_2 remain trapped underground for the foreseeable future. Careful site selection and effective injection methods are the two primary means of addressing this concern, and an accurate understanding of the subsurface spreading and migration of the CO_2 plume during and after injection is essential for both purposes. It is well known that some CO_2 will be trapped in the pore space of the aquifer rock as the plume migrates and spreads; this phenomenon, known as capillary trapping, is an ideal mechanism for geological CO_2 storage because the trapped gas is immobile and distributed over a large area, greatly decreasing the risk of leakage and enhancing the effectiveness of slower, chemical trapping mechanisms. Here, we present an analytical model for the post-injection spreading of a plume of CO_2 in a saline aquifer, both with and without capillary trapping. We solve the governing equation both analytically and numerically, and a comparison of the results for two different initial plume shapes demonstrates the importance of accounting for the true initial plume shape when capillary-trapping effects are considered. We find that the plume volume converges to a self-similar, power-law trend at late times for any initial shape, but that the plume volume at the onset of this late-time behavior depends strongly on the initial shape even for weakly trapping systems.

Thesis Supervisor: Ruben Juanes
Title: Assistant Professor, Civil and Environmental Engineering

Thesis Reader: Anette E. Hosoi
Title: Associate Professor, Mechanical Engineering

Acknowledgments

I am grateful to my research advisor, Ruben Juanes, for his guidance; to my academic advisor, Anette "Peko" Hosoi, for her enthusiasm; to my friends & fellow students, among them Fancois-Xavier Dub, Antone Jain, Michael Szulczewski, Tony Yu, Randy Ewoldt, and many others, for their camaraderie and occasional commiseration; to my girlfriend, Lindsey Morse, for her encouragement; and to my parents, Steve and Donna MacMinn, and brothers, Jon, Michael, and David MacMinn, for their confidence in my abilities.

Contents

List of Figures

Chapter 1

Introduction

Storage of carbon dioxide in geological formations is widely regarded as a promising tool for reducing global atmospheric CO_2 emissions (see, *e.g.*, [3, 18, 27, 25, 13]). Given the environmental and health risks associated with leakage of CO_2 from such a subsurface storage site, as well as the significant capital investment and other implementation costs associated with a large-scale sequestration project, it is critical to ensure that injected CO_2 remain trapped underground for the foreseeable future. Careful site selection and effective injection methods are the two primary means of addressing this concern, and an accurate understanding of the subsurface spreading and migration of the plume of mobile CO_2 during and after injection, including its shape, size, and extent, is essential for both purposes.

1.1 Saline Aquifers and Trapping Mechanisms

Among the geological formations well-suited for use as storage sites are deep saline aquifers (see, *e.g.*, [3, 25, 13])—geologic layers of permeable rock located 1 to 3 km below the surface, saturated with salty groundwater, and, in general, bordered on top by a region of much less permeable "caprock". At reservoir conditions in such an aquifer, CO_2 is less dense than the resident groundwater, and will migrate upward due to buoyancy and spread along the top boundary of the aquifer during and after injection. When upward migration of mobile CO_2 is blocked by an impermeable layer,

it is said to be *structurally* trapped, as illustrated in Figure 1-1. Structural trapping is effective but unreliable, as the CO_2 remains mobile—a pre-existing well or the activation of a fault could lead to leakage into shallower formations.

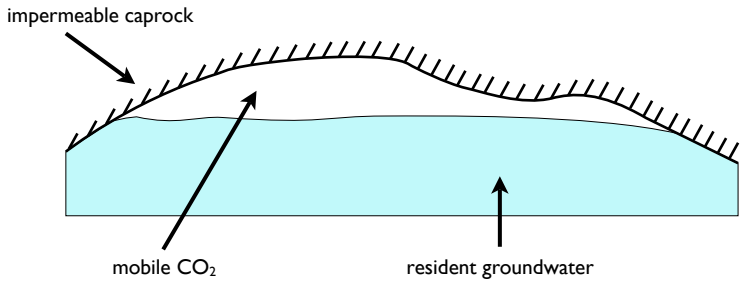

Figure 1-1: Structural trapping of CO_2 in a saline aquifer leads to a mobile plume of CO_2, the migration of which is blocked by the caprock only.

However, it is well-known that some amount of CO_2 will be trapped in the pore space of the aquifer rock at the trailing edge of the plume as it migrates and spreads [13, 15]. This phenomenon, known as capillary trapping, occurs in any porous medium when a wetting fluid (in this case, groundwater) displaces a non-wetting one (in this case, CO_2) from the pore space of the rock (*i.e.*, during imbibition). Capillary trapping, as illustrated in Figure 1-2, occurs as the wetting fluid takes the place of the non-wetting fluid because capillarity drawns the wetting fluid preferentially into smaller pore spaces before larger ones and causes pre-existing films of wetting fluid to snap off [19]. This capillarity-induced invasion causes some of the non-wetting fluid, left behind in the larger pore spaces, to be separated from the bulk; the pressure gradient in the surrounding wetting fluid can then be insufficient to displace this residual non-wetting fluid, leaving it trapped. An analogous phenomenon occurs when wetting fluid is displaced from the pore space by non-wetting fluid (*i.e.*, during drainage)—some *connate* wetting fluid is left behind in small pore spaces, immobilized by capillarity. The fraction of pore space occupied by trapped or *residual* CO_2 after the bulk is displaced is known as the residual gas saturation, denoted here as S_{gr}; similarly, the fraction of pore space occupied by connate groundwater is known as the

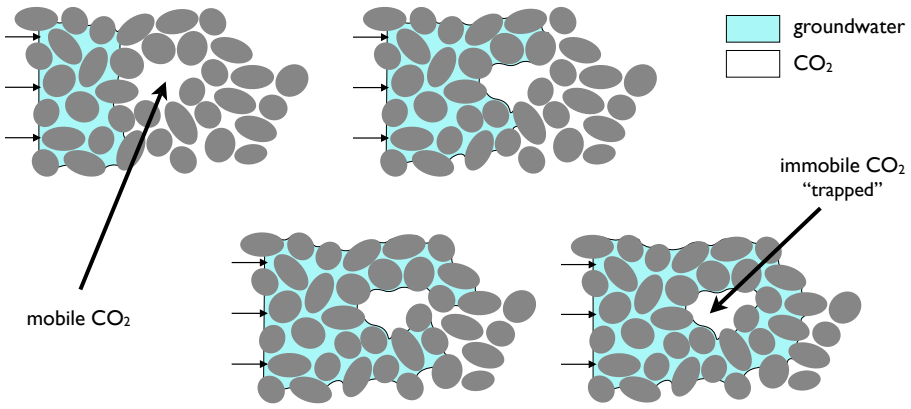

Figure 1-2: Capillary trapping occurs as the non-wetting fluid (here, CO_2) is displaced from the pore space by the wetting fluid (here, groundwater), and leads to small, disconnected regions of non-wetting fluid dispersed throughout the region from which the bulk was displaced.

connate water saturation, denoted here as S_{wc}.

One measure of the amount of capillary trapping in a system is the ratio of the residual CO_2 saturation, S_{gr}, to the initial CO_2 saturation within the plume; because the CO_2 is injected into an aquifer that initially contains only groundwater, this initial saturation is $1 - S_{wc}$. We denote this ratio the capillary trapping number, Γ:

$$\Gamma = \frac{S_{gr}}{1 - S_{wc}}. \tag{1.1}$$

Note that Γ takes a value between zero (no trapping) and one.

Capillary trapping is an ideal mechanism for the geological storage of CO_2 because the trapped gas is immobile and distributed over a large area, greatly decreasing the risk of leakage and enhancing the effectiveness of slower, chemical trapping mechanisms such as dissolution and mineral deposition. Because capillary trapping occurs at the imbibition front behind the CO_2 plume [15], it serves to couple the shape and size of the CO_2 plume to its path or "sweep" through the aquifer.

1.2 Previous Work

The injection of mobile CO_2 into a saline aquifer and its subsequent migration falls into the broad class of fluid-mechanics problems known as viscous gravity currents, wherein a finite amount or flux of one fluid is released into a second, ambient fluid. The introduced fluid having a different density than the ambient fluid, the flow is governed by the balance of buoyancy and viscosity.

Several cases of a fluid being released or injected into a less dense ambient fluid on a flat surface were considered by Huppert [11] for both planar and axisymmetric geometries; see references therein for earlier work on gravity currents. Barenblatt [5] considered a similar axisymmetric problem, the primary difference being that the flow occurred in a porous medium. This introduces several additional complications; of primary interest here is that of capillary trapping, which causes the total volume of mobile fluid in the "mound" to decrease as it slumps; Barenblatt does not consider capillary trapping in this early work. Kochina *et al.* [17] solve the same axisymmetric problem with capillary trapping; Barenblatt [4] describes the solution to the problem in both cases. More recently, Anderson *et al.* [1] extend the work of Barenblatt [5] for the planar case without capillary trapping to slumping problems with spatially periodic intrinsic permeability fields using homogenization techniques; Lyle *et al.* [20] revisit the work of Huppert [11] for the axisymmetric case, now in a porous medium but again without capillary trapping; Pritchard [26] considers planar slumping in a porous medium where the bottom boundary is fractured, leading to downward leakage.

In the problem of geological CO_2 storage, as in the problem considered by Barenblatt and Kochina, the injection and the subsequent spreading and migration of the introduced fluid occur in a porous medium. The difference is that in geological CO_2 storage, the introduced fluid is *less* dense than the ambient fluid, and it spreads along the top boundary of the domain rather than slumping along the bottom boundary. Such systems have been considered by Dussan and Auzerais [7], and by Huppert and Woods [12]. Dussan and Auzerais [7] consider the problem of drilling through a

porous layer, where drilling fluid tends to escape into the layer and propagate into the denser resident fluid; their problem is again axisymmetric, and they do not include capillary trapping. Huppert and Woods [12] consider the exchange flow between adjacent reservoirs separated by a vertical boundary that is suddenly removed in the context of a planar porous layer; capillary trapping is again neglected.

On the specific topic of the geological storage of CO_2 in a saline aquifer, Norbotten *et al.* [23] develop a governing equation for the shape of an axially symmetric CO_2 plume during injection, giving an explicit analytical solution for the case when advective viscous effects dominate diffusive buoyancy effects, which is often the case during the injection period; they demonstrate favorable comparison of their results with numerical simulations. The injection case is pure drainage when buoyancy effects are neglected, and therefore capillary trapping does not play a role. Nordbotten and Celia [24] show a different development of the same governing equation for the injection period, giving again the explicit analytical solution for the advection-dominated flow, and then proceed to integrate dissolution effects with very good agreement between analytical and numerical results.

Hesse *et al.* [10] consider the post-injection spreading and migration of the CO_2 in a planar geometry, developing a similar governing equation, now accounting for capillary trapping in the form of both connate water and trapped CO_2; Hesse *et al.* [10] develop scaling laws for the plume volume, maximum thickness, and extent in this case. Also, Hesse *et al.* [9] develop early- and late-time similarity solutions for the same problem without capillary trapping. In both cases, the authors argue that an arbitrary initial condition will give good results for late times because the system is diffusive in nature, and will therefore lose information about the initial conditions over time; they therefore choose a "step" or "square" initial condition for convenience. While it is true that the diffusive nature of the spreading process will lead to independence from initial conditions at late times when capillary trapping is not considered, we expect the initial shape of the plume to be important when the effects of capillary trapping are included—this is because the amount of CO_2 that is trapped depends directly on the so-called "sweep" of the plume as it spreads. This

point is demonstrated by Kochina *et al.* [17] and subsequently by Barenblatt [4] in the analytical solution to the slumping problem. Barenblatt [4] emphasizes that the inclusion of capillary trapping leads to a strong dependence on initial conditions that is absent when capillary trapping is not considered.

Juanes and MacMinn [14] model the planar post-injection migration of a CO_2 plume for the case where advection due to natural groundwater flow dominates diffusive spreading due to buoyancy, including the effect of capillary trapping and rigorously accounting for the true end-of-injection shape of the plume.

Here, we model the radial post-injection diffusive spreading of a CO_2 plume with no regional groundwater flow, including the effect of capillary trapping and rigorously accounting for the end-of-injection plume shape. Our aim is to show that while the solution to the spreading problem for any arbitrary initial condition converges to a universal self-similar solution when trapped gas is not included, the inclusion of capillary trapping breaks this universality and solutions are no longer independent of the initial shape of the plume. In Chapter 2, we follow [24, 10, 9] in developing a governing equation for the axially symmetric injection and spreading of a plume of CO_2 in a saline aquifer, examining in detail the validity of the underlying assumptions. In Chapter 3, we follow [23, 24] in developing a similarity solution for this governing equation for the injection period. In Chapter 4, we consider the post-injection period and develop late-time analytical solutions to the governing equation following [4] without and with the effects of capillary trapping, comparing the results for two different initial conditions. In Chapter 5, we give some concluding remarks.

Chapter 2

Development of the Analytical Model

We seek to develop a governing equation to describe the axially symmetric spreading and migration of CO_2 in a deep saline aquifer during and after injection. In this chapter, we detail the derivation of this governing equation.

Following [24, 10, 9], we employ a sharp-interface model, take advantage of the Dupuit or "vertical equilibrium" approximation, and neglect capillarity relative to buoyancy and viscosity.

2.1 Modeling Approximations

We describe here the assumptions and simplifications that will determine the form in which we will write the basic equations of fluid flow in the aquifer.

2.1.1 Aquifer Characteristics

Deep saline aquifers are appealing targets for geological CO_2 storage for a variety of reasons, including their low economic value, relatively high permeability, and large estimated worldwide storage capacity [2, 13, 27]. As described in Chapter 1, deep saline aquifers are permeable layers of rock bordered on top by a region of much less

permeable "caprock", 1 to 3 km below the surface, and saturated with salty groundwater. Deep saline aquifers are typically thin compared to their in-plane dimensions, which is to say that the typical length scale L in any horizontal direction is typically much larger than the typical length scale H in the vertical direction, $L \gg H$.

We begin by approximating the aquifer as horizontal, rigid (*i.e.*, having a rock compressibility of zero; see, *e.g.*, [6]), homogenous, and isotropic. We can then take the porosity ϕ and intrinsic permeability k of the aquifer to be uniform and constant. Further, we assume the aquifer is sufficiently large in its horizontal dimensions that edge effects are negligible, so that injected CO_2 does not "see" the outer boundaries of the domain.

Lastly, we take the upper and lower boundaries of the aquifer to be effectively impermeable, or having permeabilities much lower than that of the aquifer itself.

2.1.2 Fluid Properties

We take the two fluids to be incompressible and Newtonian, therefore having constant and uniform density and viscosity, respectively. While we recognize that, realistically, some CO_2 will dissolve into the groundwater and vice-versa, solubility effects are limited to the regions where the two fluids are in contact with one-another, which are very small compared to the total bulk volume, and we therefore neglect these effects.

2.1.3 Sharp-Interface Approximation

In general, immiscible displacement in a porous medium involves gradients in saturation—that is, there is not a sharp interface between the two fluids, but rather a mixing front of nonzero thickness across which the saturation of the displacing (displaced) fluid decreases from one to zero (zero to one). Note that this is Darcy-scale mixing—the two fluids remain immiscible at the pore scale.

When the thickness of the mixing front is small relative to other relevant flow length scales, as is often the case for geological flows, the mixing front can be treated as a sharp interface; this is known as a sharp-interface approximation, and we take

advantage of it here [6].

We therefore divide the domain into three regions, each of uniform CO_2 and groundwater saturation, with discontinuous saturations across region-region boundaries. As illustrated in Figure 2-1, region 1 contains mobile CO_2 with a saturation S_{wc} of connate groundwater, region 2 contains mobile groundwater with a saturation S_{gr} of trapped CO_2, and region 3 contains mobile groundwater with no CO_2. The aquifer has a total thickness H, and the thickness of region i, $i = 1, 2, 3$, at a radial position r and time t is denoted $h_i(r, t)$, where r is measured from the axis of symmetry of the plume. Gravity acts downward.

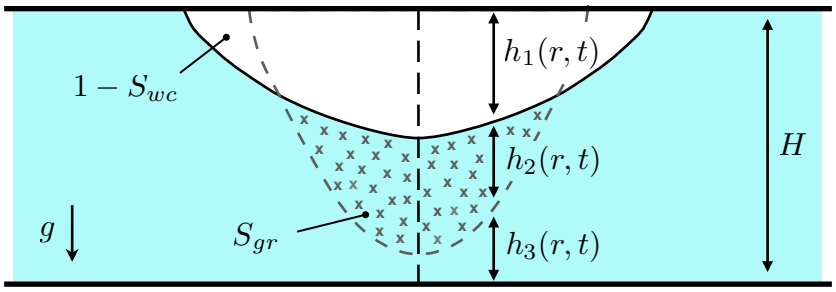

Figure 2-1: The domain is divided into three regions of uniform CO_2 and groundwater saturation separated by sharp interfaces corresponding to saturation discontinuities. Region 1 (white) has a saturation $1 - S_{wc}$ of mobile CO_2 with a saturation S_{wc} of connate groundwater; region 2 (blue with gray exes) has a saturation S_{gr} of trapped CO_2 and a saturation $1 - S_{gr}$ of mobile groundwater; region 3 (blue) contains only mobile groundwater. The plume is axially symmetric about the injection well, indicated by the vertical dashed black line. The profile of the plume at an earlier time is also shown, outlined in dashed gray.

2.2 Darcy Equations

With the approximations of Section 2.1 in mind, we can now write the Darcy velocity for each phase in each region: in region 1,

$$\boldsymbol{u}_{w1} = 0 \tag{2.1a}$$

$$\boldsymbol{u}_{g1} = -k\lambda_{g1}\nabla(p_{g1} + \rho_g g z); \tag{2.1b}$$

in region 2,

$$\boldsymbol{u}_{w2} = -k\lambda_{w2}\nabla(p_{w2} + \rho_w g z) \tag{2.2a}$$

$$\boldsymbol{u}_{g2} = 0; \tag{2.2b}$$

and in region 3,

$$\boldsymbol{u}_{w3} = -k\lambda_{w3}\nabla(p_{w3} + \rho_w g z) \tag{2.3a}$$

$$\boldsymbol{u}_{g3} = 0. \tag{2.3b}$$

The subscripts w and g refer to groundwater (the water phase) and CO_2 (the gas phase), respectively, and the subscripts 1, 2, and 3 refer to regions 1, 2, and 3, respectively, from Figure 2-1, so that $\boldsymbol{u}_{w3}$, for example, refers to the *specific discharge* or *Darcy* velocity of the water phase in region 3; $\lambda = k_r/\mu$ is the phase *mobility*, where k_r and μ are the corresponding phase *relative permeability* and dynamic viscosity, respectively; p is the phase pressure; and ρ is the phase density.

The phase pressures within each region are related by

$$p_{g1} = p_{w1} + p_{c1}, \tag{2.4a}$$

$$p_{g2} = p_{w2} + p_{c2}, \tag{2.4b}$$

$$p_{g3} = p_{w3} + p_{c3}, \tag{2.4c}$$

where p_{ci}, $i = 1, 2, 3$, is the *capillary pressure* in region i.

Note that the traditional model for multiphase flow in porous media ([28, 22, 21]) takes relative permeability and capillary pressure to be functions of phase saturation (see, *e.g.*, [6]); because the phase saturations in each region here are constant via the sharp-interface approximation, relative permeability and capillary pressure are also constant in each region.

2.2.1 Vertical Flow Equilibrium (Dupuit Approximation)

We next take advantage of the fact that aquifers are typically thin relative to their in-plane dimensions to simplify Equations (2.1), (2.2), and (2.3). We give a simple scaling justification here, but a much more detailed analysis can be found in Yortsos [29] and Yortsos [30]. We define U_r and U_z to be the typical magnitudes of the radially outward component u_r and the vertical component u_z, respectively, of the velocity field. The continuity equation for axially symmetric, incompressible flow in an incompressible aquifer,

$$\frac{1}{r}\frac{\partial}{\partial r}\left(ru_r\right) + \frac{\partial u_z}{\partial z} = 0, \tag{2.5}$$

implies that the magnitude of u_z can be estimated

$$U_z \sim \frac{H}{R}U_r, \tag{2.6}$$

where H and R are typical flow length scales in the z- and r-directions, respectively. Taking a typical reservoir thickness of $H \approx 30$ m and a typical reservoir extent of $R \approx 100$ km, it is clear that $H \ll R$ and therefore that $U_z \ll U_r$, allowing us to neglect the vertical component of the velocity relative to the radial component. This is a common simplification in hydrology; it is known as a vertical flow equilibrium or *Dupuit* approximation. From (2.1), (2.2), and (2.3), we estimate

$$u_r = -k\lambda\frac{\partial p}{\partial r} \sim -k\lambda\frac{p}{R}, \tag{2.7}$$

and, further,

$$\frac{\partial p}{\partial z} \sim \frac{p}{H} \gg \frac{\partial p}{\partial r}, \tag{2.8}$$

so therefore

$$u_r \ll -k\lambda\frac{\partial p}{\partial z}. \tag{2.9}$$

We then that argue that because $u_z \ll u_r$,

$$u_z \ll -k\lambda\frac{\partial p}{\partial z}, \tag{2.10}$$

and so, writing out the expression for the z-component of the velocity for each phase in each region, we can approximate

$$u_{g1,z} = -k\lambda_{g1}\left(\frac{\partial p_{g1}}{\partial z} + \rho_g g\right) \approx 0, \tag{2.11a}$$

$$u_{w2,z} = -k\lambda_{w2}\left(\frac{\partial p_{w2}}{\partial z} + \rho_w g\right) \approx 0, \tag{2.11b}$$

$$u_{w3,z} = -k\lambda_{w3}\left(\frac{\partial p_{w3}}{\partial z} + \rho_w g\right) \approx 0. \tag{2.11c}$$

Note that the other three velocities—$\boldsymbol{u}_{w1}$, $\boldsymbol{u}_{g2}$, and $\boldsymbol{u}_{g3}$—are identically zero. Rearranging these expressions, we can then integrate the vertical pressure gradient in each region from the 1-interface to an arbitrary height z within the region. The resulting expressions are

$$p_{g1} = p_{gI} - \rho_g g\left[z - (H - h_1)\right], \tag{2.12a}$$

$$p_{w2} = p_{w3} = p_{wI} + \rho_w g\left[(H - h_1) - z\right], \tag{2.12b}$$

$$\tag{2.12c}$$

where h_1 is the total thickness of region 1 as shown in Figure 2-1, and p_{gI} and p_{wI} are the non-wetting-phase pressure and wetting phase pressure at the 1-2 interface, respectively; note that the pressure in the wetting phase is smooth across the 2-3 boundary because the trapped gas does not contribute to the hydrostatic gradient.

2.2.2 Negligible Capillarity Compared to Gravity

We next consider the typical magnitude of capillary forces relative to buoyancy or gravity forces in the system. We can estimate the magnitude of buoyancy effects as the average hydrostatic pressure gradient, Δp_{hs}, over the thickness of the aquifer,

$$\Delta p_{hs} \sim \Delta\rho g H, \tag{2.13}$$

where $\Delta\rho = \rho_w - \rho_g$. Similarly, we can estimate the magnitude of capillary effects as the typical capillary pressure, or the typical difference in pressures between the wetting and non-wetting phases,

$$\Delta p_c \sim \frac{\gamma}{\sqrt{k/\phi}}, \tag{2.14}$$

where γ is the coefficient of interfacial tension between the two fluids, and the construction $\sqrt{k/\phi}$ is commonly used in hydrology as a characteristic length of the pore scale [6]. The ratio $\Delta p_{hs}/\Delta p_c$ is commonly known as the Bond number, Bo, and gives the importance of buoyancy effects relative to capillary effects. Here, we have

$$Bo = \frac{\Delta\rho g H}{\gamma}\sqrt{\frac{k}{\phi}}. \tag{2.15}$$

A typical saline aquifer for geological CO_2 storage purposes has thickness $H = 30$ m, with intrinsic permeability and porosity of $k = 2 \times 10^{-14}$ m^2 and $\phi = 0.15$, respectively. Taking the density difference between the two fluids, in this case groundwater and CO_2, to be $\Delta\rho \approx 500$ kg/m^3, and the interfacial tension between the two fluids to be roughly $\gamma \approx 2 \times 10^{-2}$ N/m, we find that for this system, $Bo \approx 3$, a relatively large value; we are therefore justified in neglecting the capillary pressure difference between the two phases relative to typical hydrostatic pressure gradients in the system. Considering the pressures at the 1-2 interface, we can write $p_{gI} = p_{wI} + p_{cI}$, where p_{cI} is the capillary pressure at the 1-2 interface. We now neglect this capillary pressure compared to the typical magnitudes of wetting and non-wetting phase pressures, and we can therefore take

$$p_I \equiv p_{gI} = p_{wI} + p_{cI} \approx p_{wI}, \tag{2.16}$$

where we have defined a new single pressure at the interface p_I for convenience.

2.2.3 Velocity Field

We now write the radial components of the velocity for each phase in each region in terms of the single interface pressure p_I,

$$u_1 \equiv u_{g1,r} = -k\lambda_{g1}\frac{\partial p_{g1}}{\partial r} = -k\lambda_{g1}\left(\frac{\partial p_I}{\partial r} - \rho_g g\frac{\partial h_1}{\partial r}\right), \tag{2.17a}$$

$$u_2 \equiv u_{w2,r} = -k\lambda_{w2}\frac{\partial p_{w2}}{\partial r} = -k\lambda_{w2}\left(\frac{\partial p_I}{\partial r} - \rho_w g\frac{\partial h_1}{\partial r}\right), \tag{2.17b}$$

$$u_3 \equiv u_{w3,r} = -k\lambda_{w3}\frac{\partial p_{w3}}{\partial r} = -k\lambda_{w3}\left(\frac{\partial p_I}{\partial r} - \rho_w g\frac{\partial h_1}{\partial r}\right), \tag{2.17c}$$

where we have defined u_i as the r-component of the velocity of the *mobile* phase in region i, as indicated above, for convenience.

Now that we have written the velocity in each region in terms of the interface pressure p_I and the thickness of region 1, we will relate them through conservation of mass, accounting carefully for the residual fluid that crosses each interface.

2.3 Conservation of Mass

To relate the velocities and from Equations (2.17) to each other, we consider conservation of mass. In a macroscopic sense, it is clear that the total volume flow rate through a cylinder of radius r with center at the injection well should be

$$2\pi r\left(u_1 h_1 + u_2 h_2 + u_3 h_3\right) = Q, \tag{2.18}$$

where Q is the rate of injection, Q_i, during injection, and zero after injection ends.

In addition, we consider local conservation of mass within an annular, differential element in order to relate the flow through each region to the corresponding interface displacement. Considering the differential element shown in Figure 2-2(a), we can relate the flow of mobile gas through the element with the local increase in the

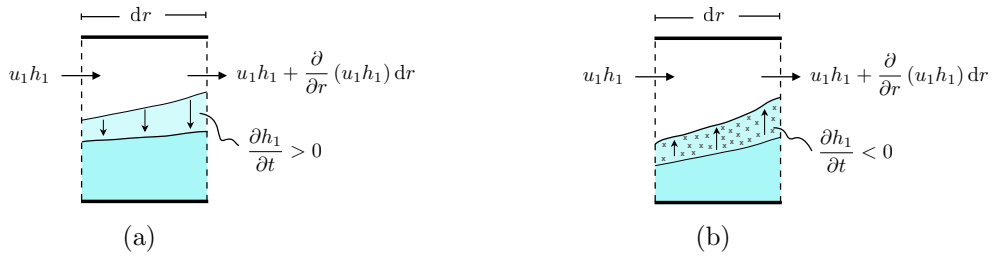

Figure 2-2: We consider flow through a cross-section of an annular differential element of the aquifer in order to relate a local change in fluid velocity to a local displacement of the interface. Here, we consider a local (a) increase and (b) decrease in the thickness h_1 of region 1 and the corresponding change in flow of mobile gas through region 1.

thickness of region 1 as

$$2\pi r\,(u_1h_1) - 2\pi\,(r+\mathrm{d}r)\left(u_1h_1 + \frac{\partial}{\partial r}\,(u_1h_1)\,\mathrm{d}r\right) = 2\pi \mathrm{d}r\,(1-S_{wc})\,\phi\frac{\partial h_1}{\partial t}, \qquad (2.19)$$

and, similarly, we can relate the flow of mobile gas through the element with the local decrease in the thickness of region 1 as

$$2\pi r\,(u_1h_1) - 2\pi\,(r+\mathrm{d}r)\left(u_1h_1 + \frac{\partial}{\partial r}\,(u_1h_1)\,\mathrm{d}r\right) = 2\pi \mathrm{d}r\,(1-S_{wc}-S_{gr})\,\phi\frac{\partial h_1}{\partial t}. \qquad (2.20)$$

Simplifying Equations (2.19) and (2.20), we can rewrite the two equations as a single conditional equation,

$$-\frac{1}{r}\frac{\partial}{\partial r}\,(r\,u_1h_1) = \begin{cases} (1-S_{wc})\,\phi\dfrac{\partial h_1}{\partial t}\,, & \dfrac{\partial h_1}{\partial t} > 0, \\ \\ (1-S_{wc}-S_{gr})\,\phi\dfrac{\partial h_1}{\partial t}\,, & \dfrac{\partial h_1}{\partial t} < 0. \end{cases} \qquad (2.21)$$

2.4 Governing Equation

Combining Equations (2.17) with (2.18), we find an expression for p_I in terms of h_1, h_2, and h_3:

$$\frac{\partial p_I}{\partial r} = \left(\frac{\rho_g\lambda_1h_1 + \rho_w\lambda_2h_2 + \rho_w\lambda_3h_3}{\lambda_1h_1 + \lambda_2h_2 + \lambda_3h_3}\right)g\frac{\partial h_1}{\partial r} - \left(\frac{1}{\lambda_1h_1 + \lambda_2h_2 + \lambda_3h_3}\right)\frac{Q}{2\pi rk}. \qquad (2.22)$$

Combining now Equation (2.22) with the Equation (2.17a), we have an expression for u_1 in terms of h_1, h_2, and h_3:

$$u_1 = \left(\frac{\lambda_1}{\lambda_1 h_1 + \lambda_2 h_2 + \lambda_3 h_3} \right) \frac{Q}{2\pi r} - \Delta\rho g k \lambda_1 \left(\frac{\lambda_2 h_2 + \lambda_3 h_3}{\lambda_1 h_1 + \lambda_2 h_2 + \lambda_3 h_3} \right) \frac{\partial h_1}{\partial r}, \tag{2.23}$$

where $\Delta\rho = \rho_w - \rho_g$. Finally, combining Equation (2.23) with (2.21), we have a governing equation for the system:

$$\tilde{\mathcal{R}} \frac{\partial h_1}{\partial t} + \frac{Q}{2\pi(1 - S_{wc})\phi} \frac{1}{r} \frac{\partial}{\partial r}\Big(f_1\Big) - \frac{\Delta\rho g k \lambda_1}{(1 - S_{wc})\phi} \frac{1}{r} \frac{\partial}{\partial r} \left((1 - f_1)\ r\, h_1 \frac{\partial h_1}{\partial r} \right) = 0, \tag{2.24a}$$

$$\tilde{\mathcal{R}} = \begin{cases} 1\,, & \frac{\partial h_1}{\partial t} > 0, \\ 1 - \Gamma\,, & \frac{\partial h_1}{\partial t} < 0, \end{cases} \tag{2.24b}$$

$$f_1 = \frac{\lambda_1 h_1}{\lambda_1 h_1 + \lambda_2 h_2 + \lambda_3 h_3}. \tag{2.24c}$$

Recall that Γ is the capillary trapping number, as defined in Equation (1.1). Equations (2.24) describe a single governing equation in three unknowns, where h_1 appears explicitly in Equation (2.24a) and dependency on h_2 and h_3 enters implicitly through the function f_1, defined in (2.24c). The set of equations describing the dynamics of the system is completed with two more relationships between h_1, h_2, and h_3; the first of these is supplied by the simple fact that the three thicknesses must sum to the total thickness of the aquifer,

$$h_1 + h_2 + h_3 = H. \tag{2.25}$$

The second relationship between h_1, h_2, and h_3 comes from the observation that a change in h_1 must correspond to a change in either h_2 or h_3, but not both—that is, a local increase in h_1 must always correspond to a local decrease in h_3, because we expect h_1 to increase only in regions where $h_2 = 0$ for a physical solution (see, *e.g.*, Figure 2-2(a)). Similarly, a local decrease in h_1 must always correspond to a local increase in h_2, because gas is trapped as the 1-2 interface is displaced toward region 1

(see, *e.g.*, Figure 2-2(b)). Mathematically, we write these requirements as

$$\frac{\partial h_1}{\partial t} = \begin{cases} -\dfrac{\partial h_2}{\partial t}, & \dfrac{\partial h_1}{\partial t} < 0, \\ \\ -\dfrac{\partial h_3}{\partial t}, & \dfrac{\partial h_1}{\partial t} > 0. \end{cases} \tag{2.26}$$

Equations (2.24), (2.25), and (2.26), taken with appropriate initial and boundary conditions, now form a complete set of three equations in three unknowns describing the dynamics of the system.

Note that Equation (2.24a) is a nonlinear advection-diffusion equation, where the advective term is driven by injection and the diffusive term is driven by buoyancy.

Chapter 3

Solution for the Injection Period

In this chapter, we consider the solution to the governing system of equations for the injection period. This result is not new—the procedure here is similar to that of Nordbotten *et al.* [24]—but we include it here for completeness.

We begin by writing the governing equation in non-dimensional form in order to compare the relative magnitudes of the advective and diffusive terms. We then neglect the diffusive term and develop an explicit analytical similarity solution to the simplified equation.

3.1 Scaling the Governing Equation

We first choose characteristic length and time scales for the system. We choose the characteristic length scale in the vertical direction to be H, and we choose the characteristic time scale t_c to be the time it takes to inject a volume V_0 of CO_2 into the aquifer at a rate of injection Q_i, so that $t_c = V_0/Q_i$. We then choose the characteristic length scale in the radial direction to be r_0, defined as the radius of a cylinder of aquifer with height H that contains a volume V_0 of CO_2, so that $V_0 = (1 - S_{wc})\phi\pi r_0^2 H$. With these definitions, we rewrite Equation (2.24a) as

$$\tilde{\mathcal{R}}\frac{\partial \eta_1}{\partial \tau} + \left(\frac{Q}{Q_i}\right)\frac{1}{2\xi}\frac{\partial}{\partial \xi}\Big(f_1\Big) - \left(\frac{2\Delta\rho g k \lambda_1 t_c H}{(1 - S_{wc})\phi r_0^2}\right)\frac{1}{2\xi}\frac{\partial}{\partial \xi}\left((1 - f_1)\,\xi\,\eta_1\frac{\partial \eta_1}{\partial \xi}\right) = 0. \quad (3.1)$$

Recalling from Equation (2.18) that the flow rate Q takes the value Q_i during the injection period, we simplify Equation (3.1) appropriately and rewrite the complete system, Equations (2.24), as

$$\tilde{\mathcal{R}}\frac{\partial \eta_1}{\partial \tau}+\frac{1}{2\xi}\frac{\partial}{\partial \xi}\Big(f_1\Big) - N_g\frac{1}{2\xi}\frac{\partial}{\partial \xi}\left((1-f_1)\,\xi\,\eta_1\frac{\partial \eta_1}{\partial \xi}\right) = 0, \tag{3.2a}$$

$$\tilde{\mathcal{R}} = \begin{cases} 1\,, & \frac{\partial \eta_1}{\partial \tau} > 0, \\ 1-\Gamma\,, & \frac{\partial \eta_1}{\partial \tau} < 0, \end{cases} \tag{3.2b}$$

$$f_1 = \frac{\lambda_1\eta_1}{\lambda_1\eta_1+\lambda_2\eta_2+\lambda_3\eta_3}, \tag{3.2c}$$

$$N_g = \Delta\rho g k\lambda_1\frac{2\pi H}{Q/H}, \tag{3.2d}$$

where the gravity number N_g gives the magnitude of diffusive buoyancy effects relative to advective viscous effects in this system.

3.2 Neglecting Buoyancy

We estimate the size of the gravity number by taking typical values of the relevant parameters for a deep aquifer (see, *e.g.*, [8])—$\rho_w \approx 1000$ kg/m^3, $\rho_g \approx 500$ kg/m^3, $k \approx 2\times10^{-14}$ m^2, $\lambda_1 \approx 2\times10^4$ Pa^{-1} s^{-1}, $H \approx 30$ m, $Q \approx 2\times10^{-2}$ m^3/s—finding that $N_g \sim 0.5$. This value is sufficiently small that buoyancy effects are much weaker than viscous effects, and the diffusive term may be safely neglected [23, 14]. This is a limit in which the thickness of region 1 is always locally increasing, meaning that $h_2 = 0$ and the system of equations is no longer conditional; we rewrite Equations (3.2) accordingly as

$$\frac{\partial \eta_1}{\partial \tau}+\frac{1}{2\xi}\frac{\partial}{\partial \xi}\Big(f_1\Big) = 0, \tag{3.3a}$$

$$f_1 = \frac{\eta_1}{\eta_1+(1-\eta_1)/\mathcal{M}}, \tag{3.3b}$$

where we have used Equation (2.25) to eliminate h_3, and the mobility ratio $\mathcal{M} = \lambda_1/\lambda_3$.

3.3 Similarity Solution

Equation (3.3) has an explicit analytical solution in the similarity parameter $\zeta = \xi^2/\tau$. Carrying out the change of variables, we find

$$\zeta = \frac{\mathrm{d}f_1}{\mathrm{d}\eta_1} = \frac{\mathcal{M}}{[(\mathcal{M}-1)\eta_1 + 1]^2}, \tag{3.4}$$

and, solving for η_1,

$$\eta_1 = \begin{cases} 1\,, & 0 \le \zeta \le 1/\mathcal{M} \\ \left(\frac{1}{\mathcal{M}-1}\right)\left(\sqrt{\frac{\mathcal{M}}{\zeta}} - 1\right), & 1/\mathcal{M} < \zeta < \mathcal{M} \\ 0\,, & \zeta \ge \mathcal{M} \end{cases} \tag{3.5}$$

Figure 3-1 shows this solution plotted at several dimensionless times for three different values of $\mathcal{M}$.

For a particular mobility ratio, Equation (3.5) can be used to find the shape of the CO_2 plume at the end of the injection period, which can then be used as an *initial condition* for the post-injection spreading of the plume.

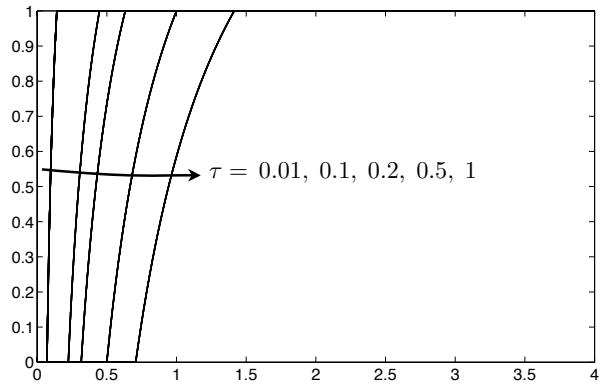

(a)

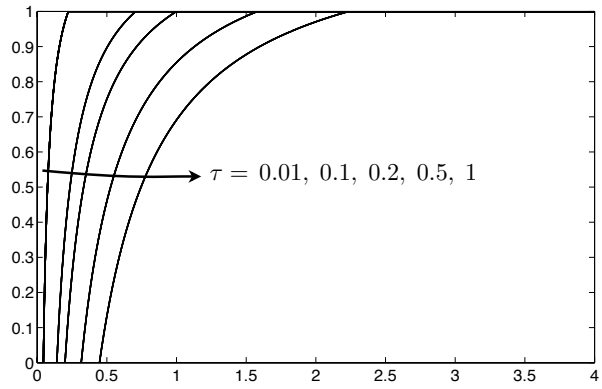

(b)

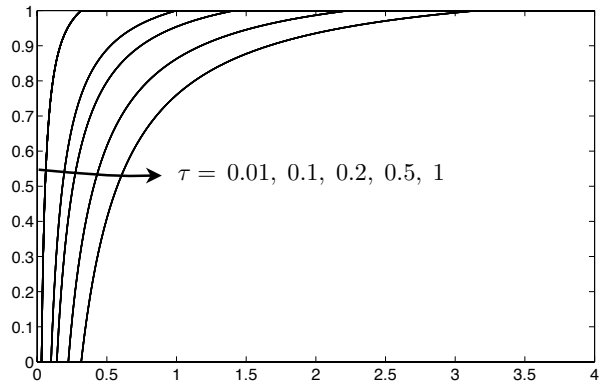

(c)

Figure 3-1: The self-similar profile of the CO_2 plume during injection, as described by Equation (3.5), is plotted for mobility ratios of (a) $\mathcal{M} = 2$, (b) 5, and (c) 10 at several dimensionless times, as indicated. The plume shape is axisymmetric about $\xi = 0$, which corresponds to the injection well. The rate of injection is constant, so the plume volume at a given time is independent of $\mathcal{M}$. Note, however, that the so-called "tonguing" of the profile increases dramatically as $\mathcal{M}$ increases.

Chapter 4

Solution for the Post-Injection Period

In this chapter, we develop an appropriate governing equation for the post-injection spreading of CO_2 in a saline aquifer. We then solve the equation analytically both without and with capillary trapping, and compare the results from two different initial conditions.

4.1 Governing Equation for CO_2 Spreading

The governing equation derived in Chapter 2 and rescaled in Chapter 3 remains valid in the post-injection period, but the injection rate Q is now zero instead of Q_i because injection has stopped. We can therefore rewrite Equation (2.24a),

$$\tilde{\mathcal{R}}\frac{\partial h_1}{\partial t} - \frac{\Delta\rho g k \lambda_1}{(1-S_{wc})\phi}\frac{1}{r}\frac{\partial}{\partial r}\left((1-f_1)\, r\, h_1 \frac{\partial h_1}{\partial r}\right) = 0. \tag{4.1}$$

In the absence of injection, we can no longer neglect the buoyancy term because it alone drives the system. We rewrite the complete governing equation one more time,

now in terms of a new parameter κ for consistency with previous work [5, 17, 4, 10],

$$\frac{\partial h_1}{\partial t} - \kappa \frac{1}{r}\frac{\partial}{\partial r}\left((1-f_1)\, r\, h_1 \frac{\partial h_1}{\partial r}\right) = 0, \tag{4.2a}$$

$$\kappa = \begin{cases} \kappa_1 = \frac{\Delta\rho g k \lambda_1}{(1-S_{wc})\phi}\,, & \frac{\partial h_1}{\partial t} > 0, \\ \kappa_2 = \frac{\Delta\rho g k \lambda_1}{(1-S_{wc}-S_{gr})\phi} = \left(\frac{1}{1-\Gamma}\right)\kappa_1\,, & \frac{\partial h_1}{\partial t} < 0, \end{cases} \tag{4.2b}$$

$$f_1 = \frac{\lambda_1 h_1}{\lambda_1 h_1 + \lambda_2 h_2 + \lambda_3 h_3}. \tag{4.2c}$$

As mentioned in Chapter 2, Barenblatt [4] describes the solution to a "slumping" problem, wherein the slumping fluid is water and the ambient fluid is a gas—in that case, the density and viscosity of the ambient fluid are neglected, and the governing equation is

$$\frac{\partial h_1}{\partial t} - \kappa \frac{1}{r}\frac{\partial}{\partial r}\left(r h_1 \frac{\partial h_1}{\partial r}\right) = 0, \tag{4.3}$$

where the coefficient κ is conditional as in (4.2). Equations (4.3) and (4.2a) have the same form because both the identities of the fluids and the direction of gravity have been reversed—that is, a lighter fluid spreading against the direction of gravity exhibits the same behavior as a heavier fluid slumping in the direction of gravity. The two equations agree exactly in the limit $f_1 \to 0$. The function f_1 does not appear in the slumping problem because the mobility of the ambient fluid is much larger than the mobility of the slumping fluid there, a limit in which $f_1 \ll 1$.

This limit does not apply to the spreading problem of interest because the mobility of the CO_2 is typically larger than that of the ambient groundwater; however, the function f_1 also becomes small when $h_1 \ll H$, *i.e.*, when the plume becomes very thin relative to the aquifer thickness, which can be considered a "late-time" regime for both problems. We therefore develop analytical solutions to Equation (4.3) without and with capillary trapping effects following [4], and these solutions then serve as asymptotics to which solutions to (4.2) tend for late times.

4.2 Spreading without Trapping, Solution for Late Times

When capillary-trapping effects are not considered, the coefficient κ in Equation (4.3) takes the constant value κ_1 and [4] shows that the equation is satisfied by a similarity solution. We detail that development here.

First, we observe that the plume thickness h_1 must be a function of time, space, the parameter κ_1, the initial volume of fluid in the plume, which we take to be V_0, and some parameter describing the initial shape of the plume, for which we take r_0 defined as before, such that $V_0 = (1 - S_{wc})\phi\pi r_0^2 H$. Thus, we write

$$h_1 = h_1(r, t, \kappa_1, \tilde{V}_0, r_0), \tag{4.4}$$

where $\tilde{V}_0 = V_0/(1 - S_{wc})\phi$ is the volume of porous medium filled by the initial fluid volume V_0, and we take the initial profile to be a cylinder or "step" with $h_1 = H$ for $r < r_0$ and $h_1 = 0$ for $r > r_0$. The dimensions of these parameters are

$$\begin{aligned} [h_1] = \mathrm{H}\,, \quad [r] = \mathrm{L}\,, \quad [t] = \mathrm{T}\,, \\ [\kappa_1] = \mathrm{L}^2\mathrm{T}^{-1}\mathrm{H}^{-1}\,, \quad [\tilde{V}_0] = \mathrm{L}^2\mathrm{H}\,, \quad [r_0] = \mathrm{L}, \end{aligned} \tag{4.5}$$

where H, L, and T here represent the dimensions of length in the vertical direction, length in the horizontal direction, and time, respectively. With six parameters and three dimensions, we expect three dimensionless groups. Proceeding with dimensional analysis, the three dimensionless or "Π" groups that govern the behavior of the system are [4],

$$\Pi_1 = h_1 \left(\frac{\kappa_1 t}{\tilde{V}_0}\right)^{1/2}, \quad \Pi_2 = r \left(\frac{1}{\tilde{V}_0 \kappa_1 t}\right)^{1/4}, \quad \Pi_3 = r_0 \left(\frac{1}{\tilde{V}_0 \kappa_1 t}\right)^{1/4}, \tag{4.6}$$

and the solution then takes the form $\Pi_1 = F(\Pi_2, \Pi_3)$. Because the problem is diffusive in nature and we are not considering capillary trapping, we seek an asymptotic solution that is independent of the initial condition to which the solution for any

arbitrary initial condition should converge—that is, we seek a solution in the limit of $\Pi_3 \to 0$ while Π_1 and Π_2 remain finite.

Proceeding with the mechanics of the similarity solution, the governing equation becomes

$$\frac{\mathrm{d}}{\mathrm{d}\Pi_2}\left\{\Pi_2 F\left[\frac{1}{4}\Pi_2 + F'\right]\right\} = 0, \tag{4.7}$$

which can be integrated directly to give

$$\Pi_1 = F(\Pi_2) = F_0 - \frac{1}{8}\Pi_2^2, \tag{4.8}$$

where the constant F_0 is determined through integral conservation of volume. Writing the full equation for h_1,

$$h_1(r,t) = \left(\frac{\tilde{V}_0}{\kappa_1 t}\right)^{1/2}\left[F_0 - \frac{1}{8}r^2\left(\frac{1}{\tilde{V}_0\kappa_1 t}\right)^{1/2}\right], \tag{4.9}$$

we calculate the volume V of CO_2 in the plume by integrating h_1 from the axis of the plume, $r = 0$, to the outer edge of the plume, which is defined as the value of r at which $h_1 = 0$ and is given by $r = r_1 = \sqrt{8F_0(\tilde{V}_0\kappa_1 t)^{1/2}}$:

$$V = (1 - S_{wc})\phi\int_0^{r_1} 2\pi r\, h_1(r,t)\,\mathrm{d}r. \tag{4.10}$$

Equating the resulting expression with the initial volume of CO_2 in the plume, V_0, we find $F_0 = 1/\sqrt{4\pi}$ and we can then write

$$h_1(r,t) = \left(\frac{\tilde{V}_0}{\kappa_1 t}\right)^{1/2}\left[\frac{1}{\sqrt{4\pi}} - \frac{1}{8}r^2\left(\frac{1}{\tilde{V}_0\kappa_1 t}\right)^{1/2}\right], \tag{4.11}$$

valid for $0 \le r \le r_1 = 2(\tilde{V}_0\kappa_1 t/\pi)^{1/4}$. We can write Equation (4.11) in dimensionless form using the scaling from Section 3.1—*i.e.*, $\eta_1 = h_1/H$, $\xi = r/r_0$, $\tau = t/t_c$, and

$\tilde{\kappa}_1 = (Ht_c/r_0^2)\kappa_1$, where $\tilde{V}_0 = \pi r_0^2 H$ as before—and the result is,

$$\eta_1(\xi,\tau) = \left(\frac{1}{\tilde{\kappa}_1\tau}\right)^{1/2}\left[\frac{1}{2} - \frac{1}{8}\xi^2\left(\frac{1}{\tilde{\kappa}_1\tau}\right)^{1/2}\right], \tag{4.12}$$

valid for $0 \leq \xi \leq \xi_1 = 2(\tilde{\kappa}_1\tau)^{1/4}$.

While the above solution was derived for a cylindrical "step" initial profile, we expect any arbitrary initial profile to converge to this solution as the details of the initial condition are lost. To demonstrate this point, we solve Equation (4.3) numerically using a finite-volume scheme for two different initial conditions—a "step" profile, and also a "true" end-of-injection profile calculated from the solution for the injection period given in Chapter 3; we take a mobility ratio of $\mathcal{M} \approx 5$, a moderate value. Note that we take the characteristic time t_c to be the length of the injection period; $\tau = 0$ corresponds to the end of injection, and each unit of dimensionless time thereafter is then one "injection time".

The spreading of the CO_2 plume without trapping is shown in Figures 4-1 and 4-2. Figure 4-1 gives the shape of the CO_2 plume at several times for both initial conditions. Figure 4-2 illustrates the spreading of the CO_2 plume without trapping by way of the time evolution of the thickness of the CO_2 plume at its axis for both initial conditions, and the convergence in both cases to the analytical solution. It is clear from Figure 4-2 that the influence of the initial conditions is lost relatively early here, and the numerical solutions then converge together to the analytical solution.

4.3 Spreading with Trapping, Solution for Late Times

When the effects of capillary trapping are included, Barenblatt [4] shows that the similarity solution above can no longer satisfy the requirement that the solution be continuous when combined with the conditional coefficient κ. Barenblatt explains

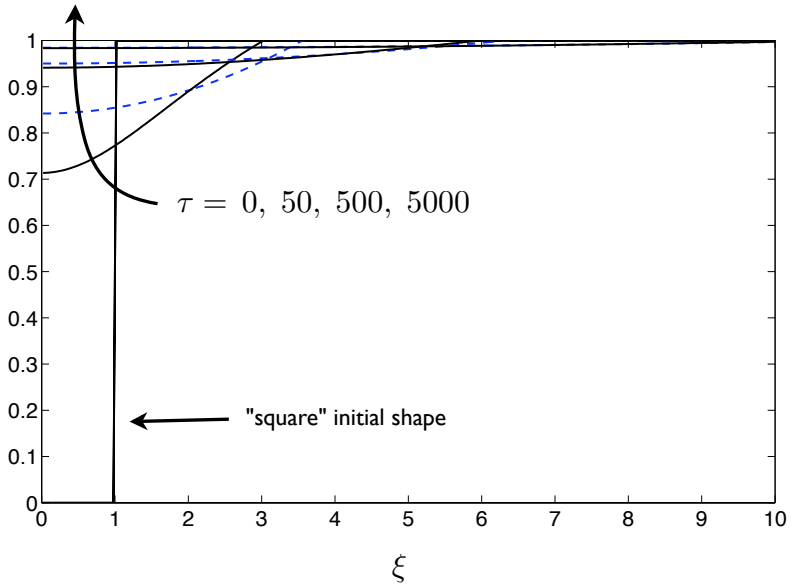

(a)

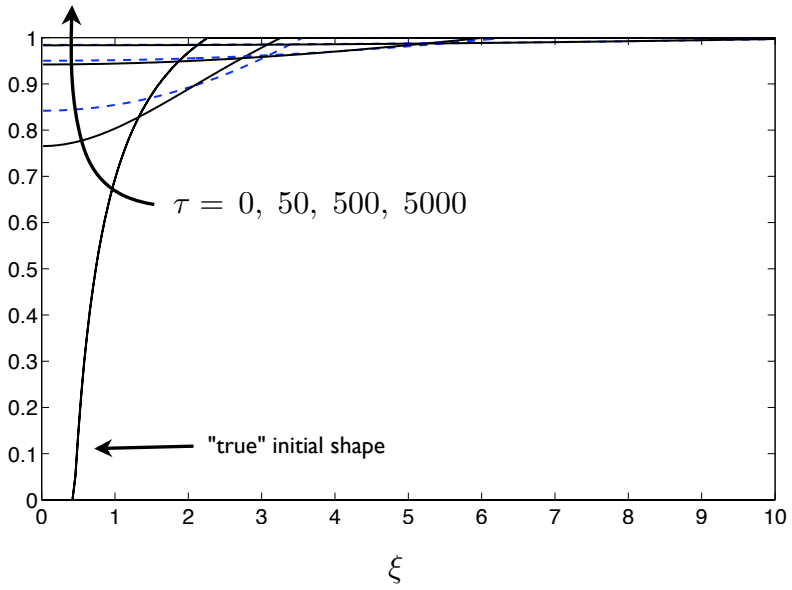

(b)

Figure 4-1: The shape of the CO_2 plume (solid black line) after spreading for 0 (initial shape), 50, 500, and 5000 injection times from the (a) "square" and (b) "true" initial conditions with no trapping. The analytical solution is also shown (dashed blue line), and the convergence of both numerical solutions toward the analytical solution is clear. Profiles are again axisymmetric about $\xi = 0$, which corresponds to the injection well.

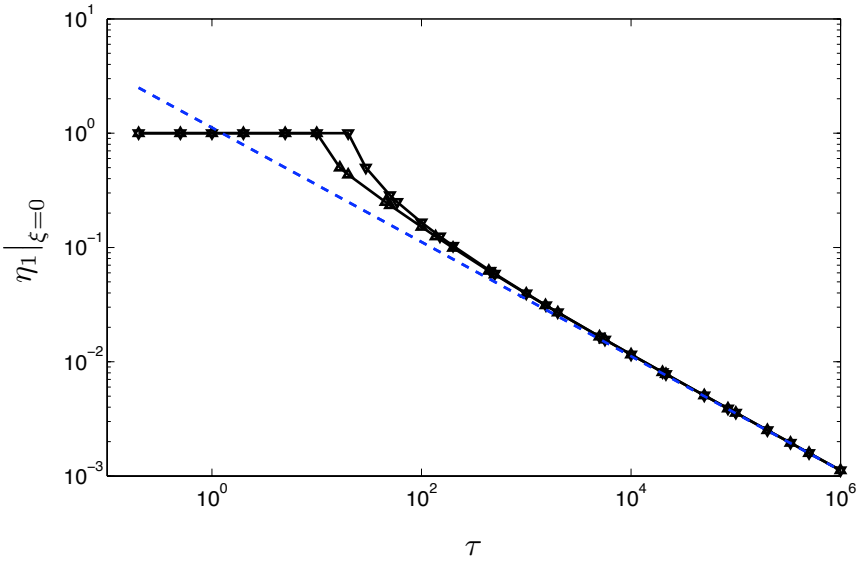

Figure 4-2: Time-evolution of the thickness of the CO_2 plume at its axis of symmetry ($\xi = 0$) without capillary trapping and for $\tilde{\kappa} = 0.2$, a reasonable value for geological CO_2 storage. Numerical solutions to the full equation (solid black lines) are shown for both "square" (downward-pointing triangle markers) and "true" (upward-pointing triangle markers) initial conditions; the analytical solution to the late-time governing equation is also shown (dashed blue line). Note that the numerical solutions for both initial conditions converge to a single late-time analytical solution.

that the reason for this is that, unlike the no-trapping case, the system never becomes completely independent of the initial state; this is evident in the structure of the solution. We detail the solution procedure here.

Performing dimensional analysis, the first three dimensionless groups are the same as before, and the ratio of the values of the conditional coefficient forms a fourth, $\Pi_4 = \kappa_1/\kappa_2 = 1 - \Gamma$ [17, 4]. As before, the group that contains information about the initial conditions is Π_3 and, as before, it will tend toward zero as time increases. In order for the system to retain information about the initial conditions, we suppose a similarity solution of the *second kind*, wherein Π_3 is no longer independent, but instead appears in conjunction with Π_1 and Π_2:

$$\frac{\Pi_1}{\Pi_3^\gamma} = F_1\left(\zeta = \frac{\Pi_2}{\Pi_3^\delta}\,,\,\Pi_4\right), \tag{4.13}$$

where γ and δ are unknown exponents to be determined in the course of the solution. Following through with the mechanics of the solution, the result, after a considerable amount of algebra, is a new system of ordinary differential equations,

$$\frac{\mathrm{d}}{\mathrm{d}\zeta}\left(F_1\frac{\mathrm{d}F_1}{\mathrm{d}\zeta}\right) + \frac{1}{\zeta}F_1\frac{\mathrm{d}F_1}{\mathrm{d}\zeta} + \left((1-2\beta)F_1 + \beta\zeta\frac{\mathrm{d}F_1}{\mathrm{d}\zeta}\right) = 0, \tag{4.14a}$$

$$\frac{\mathrm{d}}{\mathrm{d}\zeta}\left(F_1\frac{\mathrm{d}F_1}{\mathrm{d}\zeta}\right) + \frac{1}{\zeta}F_1\frac{\mathrm{d}F_1}{\mathrm{d}\zeta} + (1-\Gamma)\left((1-2\beta)F_1 + \beta\zeta\frac{\mathrm{d}F_1}{\mathrm{d}\zeta}\right) = 0, \tag{4.14b}$$

where (4.14a) and (4.14b) are valid for $((1-2\beta)F_1 + \beta\zeta\mathrm{d}F_1/\mathrm{d}\zeta) < 0$ and > 0, respectively, and the two unknown constants γ and δ have been rewritten in terms of a single unknown constant β; one unknown has been eliminated through the requirement that neither τ nor ξ can appear explicitly in Equations (4.14). Equations (4.14) form a second-order system of ODEs, the solution to which is subject to two boundary conditions:

1. No flux at the axis of the plume or, equivalently, radial symmetry of the plume shape about $\xi = 0$. Mathematically, this condition becomes:

$$\left.\frac{\partial h_1}{\partial r}\right|_{r=0} = 0 \quad \rightarrow \quad \left.F_1'\right|_{\zeta=0} = 0. \tag{4.15}$$

2. No flux at the outer edge of the plume, because we require that the flux vary smoothly to zero there. Mathematically, we write this requirement

$$h_1 \frac{\partial h_1}{\partial r}\bigg|_{r=r_1} = 0 \quad \rightarrow \quad F_1 F_1'\bigg|_{\zeta=\zeta_1} = 0. \tag{4.16}$$

However, as previously, we define $r = r_1$ as the value of r at which $h_1 = 0$ and, similarly, we define $\zeta = \zeta_1$ as the value of ζ at which $F_1 = 0$; this boundary condition is therefore satisfied automatically. Instead, we must ensure that the parameter ζ_1 satisfies the governing equations. Evaluating Equations (4.14) at $\zeta = \zeta_1$, we find that this requires that

$$F_1'\bigg|_{\zeta=\zeta_1} = -\beta\zeta_1. \tag{4.17}$$

This is our second boundary condition.

Two boundary conditions, however, are insufficient—the parameter β is a third unknown. Lack of a third boundary condition leaves one degree of freedom in the system and, as in the no-trapping case, this is set by the volume of mobile gas in the plume at the time when the spreading behavior becomes self-similar. Unlike the no-trapping case, however, this condition cannot be applied as an analytical integral, and must instead be extracted from a numerical solution to the full governing equation.

We proceed as follows: first, we let the value of ζ corresponding to the outer edge of the plume, ζ_1, be equal to 1—this choice scales the shape of the plume, and we will rescale it appropriately at the end. Second, we guess a value of β and solve Equations (4.14) numerically starting at $\zeta = \zeta_1 = 1$, where the value of F_1 is zero by the definition of ζ_1 and the slope of F_1 is set by the second boundary condition above; we solve from $\zeta = \zeta_1$ to $\zeta = 0$ using a shooting method [16]. Third, we check whether or not this solution satisfies the first boundary condition above, which is a constraint on the slope of F_1 at $\zeta = 0$—if not, we update our guess for β accordingly and iterate. The solution to Equations (4.14) for a particular value of the capillary trapping number Γ is then both the function F_1 and also the particular value of β

for which this function satisfies the boundary conditions; β is then an eigenvalue of the system. We solve Equations (4.14) over the range of values of Γ, and present the results in Figure 4-3 below.

In order to reconcile this solution with the physical system, we must now match it with a numerical solution to the full system. In Equation (4.13), we proposed a solution of the form

$$h_1 = \left(\frac{r_0^2}{\kappa_1 t}\right)\left(\frac{\tilde{V}_0\kappa_1 t}{r_0^4}\right)^{2\beta} F_1\left(\zeta = \frac{r}{r_0}\left(\frac{r_0^4}{\tilde{V}_0\kappa_1 t}\right)^{\beta}, \Gamma\right). \tag{4.18}$$

This form is no longer valid because of our arbitrary choice of $\zeta_1 = 1$; we must therefore rescale the parameter ζ to correct for this choice, lumping the constants together into a single new parameter B,

$$\zeta = \frac{r}{r_0}\left(\frac{r_0^4}{\tilde{V}_0\kappa_1 t}\right)^{\beta} \quad \rightarrow \quad \zeta = \frac{r}{Bt^{\beta}}. \tag{4.19}$$

We group the constants outside the function F_1 in Equation (4.18) similarly for consistency, finding that

$$\left(\frac{r_0^2}{\kappa_1 t}\right)\left(\frac{\tilde{V}_0\kappa_1 t}{r_0^4}\right)^{2\beta} \quad \rightarrow \quad \frac{1}{\kappa_1 t}\left(Bt^{\beta}\right)^2, \tag{4.20}$$

and we now have a solution of the form

$$h_1 = \frac{1}{\kappa_1 t}\left(Bt^{\beta}\right)^2 F_1\left(\zeta = \frac{r}{Bt^{\beta}}, \Gamma\right). \tag{4.21}$$

Our last step is then to solve the full spreading equation numerically until the spreading behavior becomes self-similar, and choose the value of B appropriately so that the mobile gas volume of the self-similar analytical solution at this point matches that of the full numerical solution. The final analytical solution then describes the spreading behavior at times after it becomes self-similar—it incorporates "memory" of the initial conditions and the pre-self-similar history through the remaining mobile

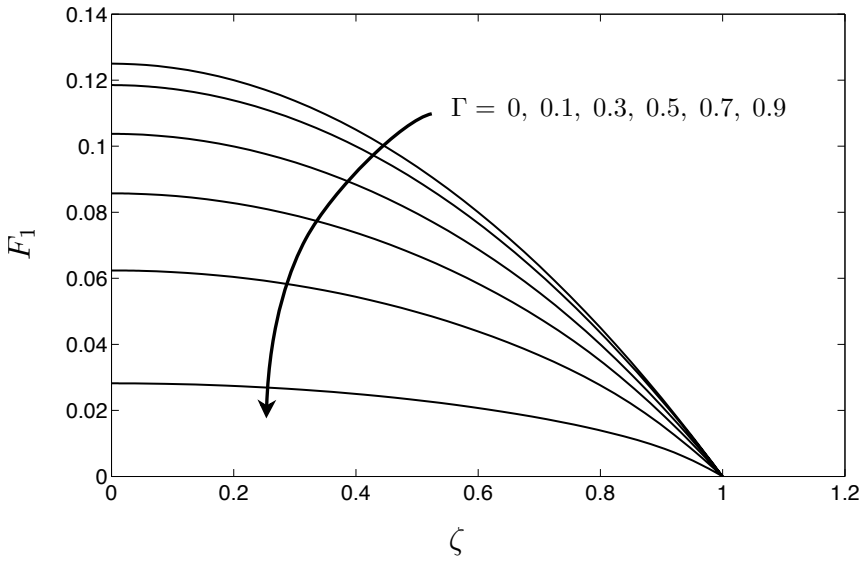

(a)

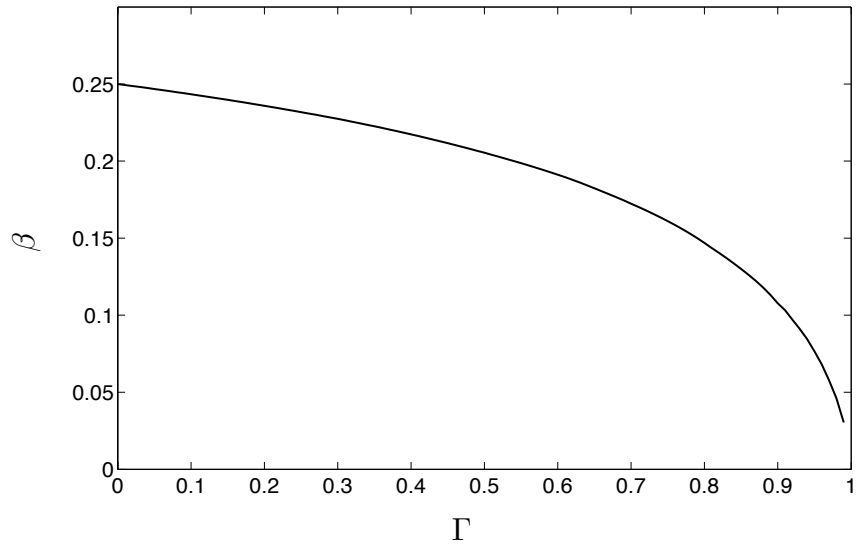

(b)

Figure 4-3: Solutions to the eigenvalue problem formed by Equations (4.14) and the two boundary conditions. We show (a) the function $F_1(\zeta)$ for several values of Γ and (b) the eigenvalue β as a function of Γ. Note that by construction, all of the functions F_1 are equal to zero at $\zeta = \zeta_1 = 1$.

gas volume at the time when self-similar behavior begins, and this remaining mobile gas volume is strongly dependent on the initial shape of the plume at the end of the injection period.

We can write the solution in dimensionless form as

$$\eta_1(\xi,\tau) = \frac{1}{\tilde{\kappa}_1\tau}\left(\tilde{B}\tau^{\beta}\right)^2 F_1\left(\zeta = \frac{\xi}{\tilde{B}\tau^{\beta}}\,,\,\Gamma\right), \tag{4.22}$$

where $\tilde{\kappa}_1$ is defined as

$$\tilde{\kappa}_1 = \left(\frac{Ht_c}{r_0^2}\right)\kappa_1, \tag{4.23}$$

as before, and the constant $\tilde{B}$ is defined as

$$\tilde{B} = \left(\frac{t_c^{\beta}}{r_0}\right)B. \tag{4.24}$$

It is clear that the spreading behavior can be characterized by two parameters: the capillary trapping coefficient Γ, which uniquely determines the function F_1 and the value of β, and the specific value of either $\tilde{\kappa}_1$ or $\tilde{\kappa}_2$.

The spreading of the CO_2 plume for typical values of the two parameters—$\tilde{\kappa}_1 = 0.2$ and $\Gamma = 0.2$, a moderate value (given by, *e.g.*, $S_{gr} = 0.15$, $S_{wc} = 0.25$)—is shown in Figure 4-4 below, which gives the shape of the CO_2 plume at several times for both initial conditions. The convergence of both numerical solutions toward the respective analytical solutions is clear. Note also the distinctly different trapped-gas envelopes between the two cases.

Figure 4-5 shows the time evolution of the plume volume, again for $\tilde{\kappa}_1 = 0.2$ and $\Gamma = 0.2$. It is clear from Figure 4-5 that the two solutions do indeed converge to the same late-time *trend* or *scaling*, but remain separated by a significant "gap" in volume at a particular time, or a "gap" in time at a particular volume—for these parameters, for example, it takes roughly five times longer for the mobile plume volume to decrease to a particular value for the "true" initial condition than it does for the plume volume to decrease to the same value for the "square" initial condition. This gap results from

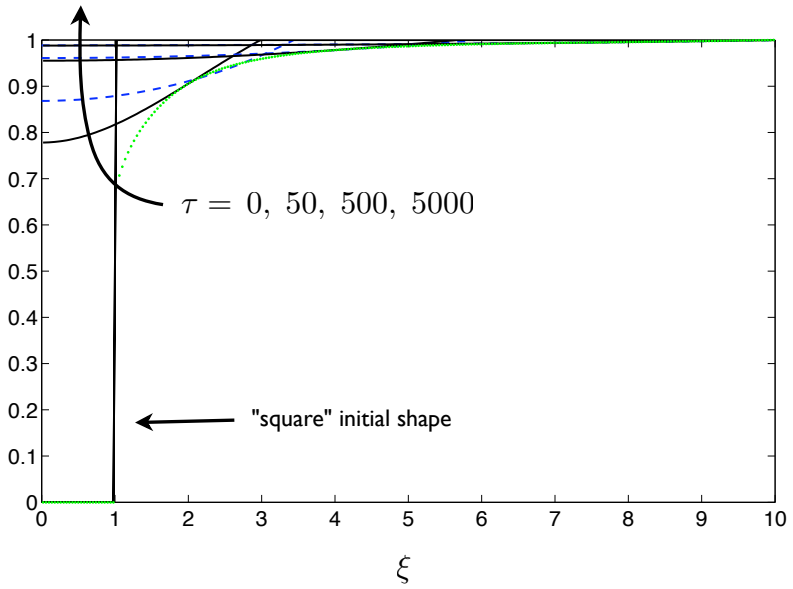

(a)

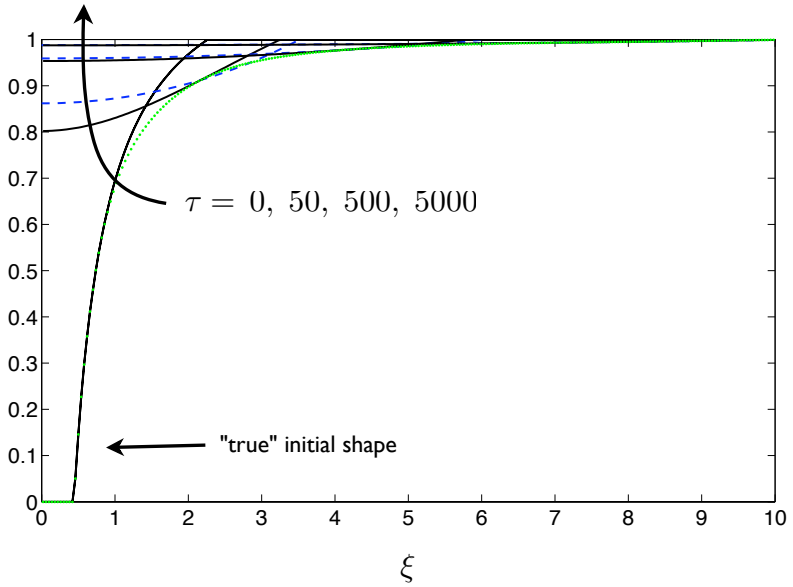

(b)

Figure 4-4: The shape of the CO_2 plume (solid black line) after spreading for 0 (initial shape), 50, 500, and 5000 injection times from the (a) "square" and (b) "true" initial conditions with moderate trapping ($\Gamma = 0.2$). The envelope of the region containing mobile water and trapped gas (region 2 in Figure 2-1) after 5000 injection times is also shown (dotted green line), as well as the analytical solution (dashed blue line) after 50, 500, and 5000 injection times. Profiles are again axisymmetric about $\xi = 0$, which corresponds to the injection well. The convergence of both numerical solutions toward the respective analytical solutions is clear. Note also the distinctly different trapped-gas envelopes between the two cases.

the fact that the two different initial conditions lead to substantially different amounts of total trapped gas over the course of the transition from the initial shape to the late-time self-similar behavior, and this difference is *never recovered* despite the diffusive nature of the system.

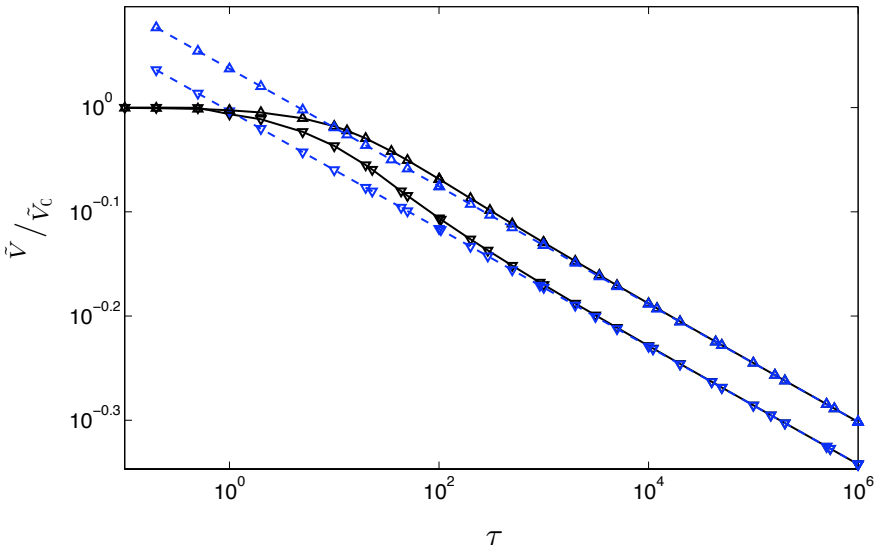

Figure 4-5: Time evolution of the volume of the CO_2 plume, scaled by its initial volume, for moderate capillary trapping ($\Gamma = 0.2$) and $\tilde{\kappa} = 0.2$. Numerical solutions to the full equation (solid black lines) and late-time analytical solutions (dashed blue lines) are shown for both "square" (downward-pointing triangle markers) and "true" (upward-pointing triangle markers) initial conditions. Note that the numerical solutions for the two different initial conditions now converge to different late-time analytical solutions, exhibiting the same late-time trend but separated by a significant gap due to different amounts of total trapped gas during the transition from the initial condition to the late-time self-similar behavior.

The result for the particular parameters shown in Figure 4-5 is typical, but the size of the "gap" depends on the capillary trapping coefficient and on the parameter $\tilde{\kappa}_1$. Figure 4-6 illustrates this dependence through the ratio of the time at which the volume of the plume reaches a particular value for the "true" initial condition to the time at which the volume of the plume reaches the same value for the "square" initial condition. Note that for no trapping, the plume volume is constant and independent of initial conditions, and this "time ratio" takes a value of 1.

It is clear from Figure 4-6 that the "time ratio" varies much more with Γ than

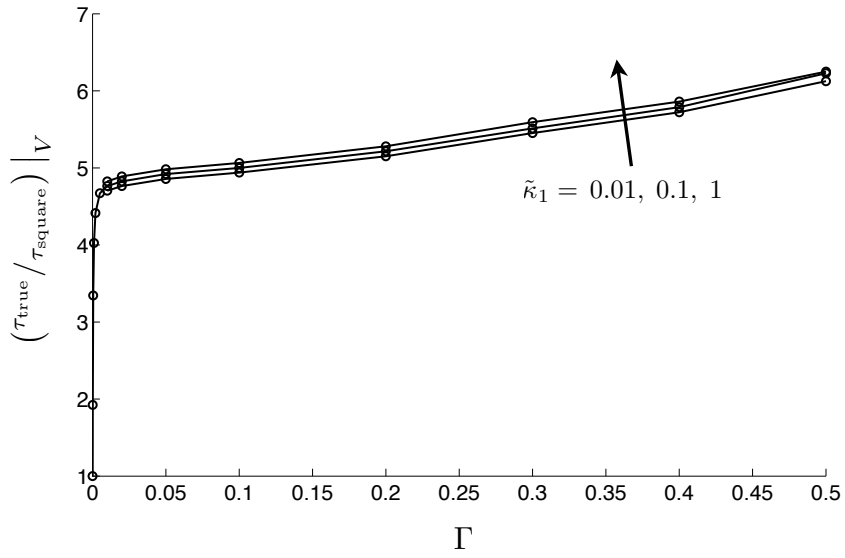

Figure 4-6: The ratio of the time at which the volume of the plume reaches a particular value for the "true" initial condition to the time at which the volume of the plume reaches the same value for the "square" initial condition, plotted for several values of $\tilde{\kappa}_1$ over a range of Γ values. Values shown are for late-time, self-similar plume evolution only, a regime in which this ratio is a constant. The time ratio here does not depend strongly on either parameter, though variation with $\tilde{\kappa}_1$ is much weaker than variation with Γ. Note, however, that even weak trapping has a significant effect—the time ratio is nearly a factor of 5 for even small values of Γ.

with $\tilde{\kappa}_1$. Note also that the time ratio takes a value of nearly 5, meaning that the plume for the "true" initial condition takes nearly five times longer than the plume for the "square" initial condition to decrease to a given volume, for even very small values of Γ. This may seem counterintuitive, because the difference between plume *volumes* at a given time for two different initial conditions decreases as the amount of trapping decreases. However, the rate of trapping also decreases as the amount of trapping decreases, so that a given gap in volume then corresponds to a larger gap in time. These competing effects lead to the behavior shown in Figure 4-6: the "time ratio" increases sharply from 1 to nearly 5 as Γ increases from 0 to 0.01, respectively, then increases more gently with Γ thereafter.

While variations in $\tilde{\kappa}_1$ have only a weak effect on the difference between initial conditions, they have a strong influence on the amount of time it takes for solutions to converge to late-time behavior. This effect is illustrated in Figure 4-7.

Because $\tilde{\kappa}_1$ is effectively a diffusion coefficient in this system, we would expect convergence time to vary inversely with changes in $\tilde{\kappa}_1$. It is clear from Figure 4-7 that this is indeed the case and, in fact, we find that this trend is very accurately described by

$$\tau^\star \sim \frac{1}{\tilde{\kappa}_1}. \tag{4.25}$$

Convergence time also varies inversely with Γ, but the effect is much weaker.

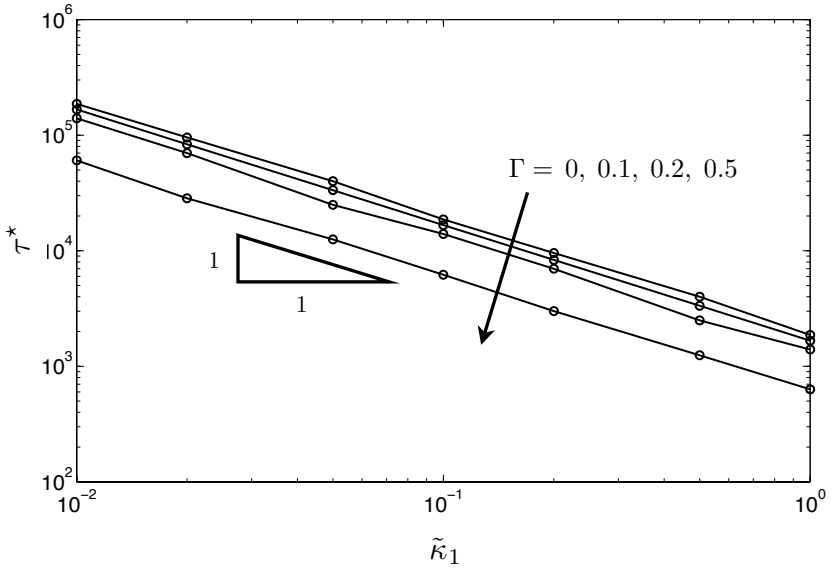

Figure 4-7: The dimensionless time $\tau^\star$ at which the numerical solution has converged to the late-time analytical solution over a range of values of the parameter $\tilde{\kappa}_1$ and for capillary trapping coefficients of, from top to bottom, $\Gamma = 0$ (no trapping), 0.1 (weak trapping), 0.2 (moderate trapping), and 0.5 (strong trapping); we find that $\tau^\star$ is almost exactly inversely proportional to $\tilde{\kappa}_1$ for all values of Γ. Results here are for a "true" initial condition; results for a "square" initial condition are qualitatively similar. We define "convergence time" here as the time at which the time-rate-of-change of the plume thickness at the origin converges to within 3% of the analytical value, and it should be noted that the magnitude of the convergence time is strongly sensitive to this choice of error margin; more stringent values than the 3% used here, for example, give qualitatively similar variation with Γ and $\tilde{\kappa}_1$, but significantly longer convergence times.

Chapter 5

Discussion and Conclusions

We have developed an analytical model for the post-injection spreading of a plume of CO_2 in a saline aquifer and, by comparing the results for two different initial conditions, have shown that the phenomenon of capillary trapping leads to a strong influence of initial conditions on this spreading behavior that is not present in the absence of capillary trapping. In particular, we have shown that even very small amounts of trapping lead to significantly different results for different initial conditions. This result implies that models for subsurface CO_2 spreading or migration should account rigorously for the true end-of-injection plume shape in order to predict plume thicknesses, volumes, or extents over time with any degree of accuracy. Figure 4-6 illustrates that different initial conditions can lead to dramatically different times for a given volume to be trapped for even very small values of the capillary trapping number; for the parameters investigated here, for example, use of a "square" initial condition rather than the "true" initial leads to the under-prediction of the time it will take a given volume of CO_2 to become trapped by a factor of 4 to 5 in even a weakly trapping system, and by a factor of more than 6 in a strongly trapping system.

It should be noted that there are two additional parameters in this system, the effects of which we have not investigated here. First, the "true" post-injection initial condition was calculated for a mobility ratio of $\mathcal{M} = \lambda_1/\lambda_3 \approx 5$, as an appropriate moderate value for a deep, cool aquifer. Second, the relative permeability to water in the region with trapped gas, region 2 in Figure 2-1, was taken here to be 1. We

expect that the difference between what we have termed early- and late-time behavior would be more pronounced with a larger mobility ratio because the magnitude of the function f_1 increases with increasing mobility ratio, as discussed in the Chapter 4; the influence of f_1 should therefore also take longer to vanish for larger mobility ratio, leading to longer convergence times $\tau^\star$. It is also clear that the difference between a "true" initial condition and a "square" initial condition will increase dramatically as the mobility ratio increases because the of the significant increase in "tonguing" discussed in Chapter 3 (see *e.g.*, [24, 14]); this effect should strengthen the dependence on initial conditions we have illustrated here.

The influence on spreading of variations in the relative permeability to water in the region with trapped gas is unclear. It is well-known that an increase in the amount of trapped gas (a larger value of Γ) will cause a decrease in the relative permeability to water in this region, and it could be argued, for example, that this "buffer zone" of decreased water mobility will serve to slow the spreading of the plume and lead to longer convergence times. If this is indeed the case, this increase in $\tau^\star$ with Γ could somewhat counter the decrease in $\tau^\star$ with Γ that we show in Figure 4-7. The exact nature and strength of this effect will depend on the specific choice of water relative permeability function for the aquifer, however, and it is therefore difficult to make general predictions. An exploration of this effect may be the subject of future work.

Bibliography

[1] D. M. Anderson, R. M. McLaughlin, and C. T. Miller. The averaging of gravity currents in porous media. *Physics of Fluids*, 15(10):2810–2829, 2003.

[2] S. Bachu. Screening and ranking of sedimentary basins for sequestration of CO_2 in geological media in response to climate change. *Environmental Geology*, 44(3):277–289, 2003.

[3] S. Bachu, W. D. Gunter, and E. H. Perkins. Aquifer disposal of CO_2: hydrodynamic and mineral trapping. *Energy Conversion and Management*, 35(4):269–279, 1994.

[4] G. I. Barenblatt. *Scaling, self-similarity, and intermediate asymptotics*. Cambridge University Press, 1996.

[5] G. I. Barenblatt, V. M. Entov, and V. M. Ryzhik. *Theory of Non-Steady Filtration of Fluids and Gases*. Nedra, Moscow, 1972.

[6] J. Bear. *Dynamics of fluids in porous media*. Courier Dover Publications, 1988.

[7] E. B. Dussan V. and F. M. Auzerais. Buoyancy-induced flow in porous media generated near a drilled oil well. Part 1. The accumulation of filtrate at a horizontal impermeable boundary. *Journal of Fluid Mechanics*, 254:283–311, 1993.

[8] A. Ebigbo, H. Class, and R. Helmig. CO_2 leakage through an abandoned well: problem-oriented benchmarks. *Computational Geosciences*, 11(2):103–115, 2007.

[9] M. A. Hesse, H. A. Tchelepi, B. J. Cantwell, and F. M. Orr. Gravity currents in horizontal porous layers: transition from early to late self-similarity. *Journal of Fluid Mechanics*, 577:363–383, 2007.

[10] M. A. Hesse, H. A. Tchelepi, and F. M. Orr. Scaling analysis of the migration of CO_2 in saline aquifers. In *SPE Annual Technical Conference and Exhibition*, number SPE 102796, San Antonio, TX, 2006. Society of Petroleum Engineers.

[11] H. E. Huppert. The propagation of two-dimensional and axisymmetric viscous gravity currents over a rigid horizontal surface. *Journal of Fluid Mechanics*, 121:43–58, 1982.

[12] H. E. Huppert and A. W. Woods. Gravity-driven flows in porous layers. *Journal of Fluid Mechanics*, 292:55–69, 1995.

[13] IPCC. Carbon Dioxide Capture and Storage. Special Report prepared by Working Group III of the Intergovernmental Panel on Climate Change, Cambridge, UK, 2005.

[14] R. Juanes and C. W. MacMinn. Upscaling of capillary trapping under gravity override: application to CO_2 sequestration in aquifers. In *SPE/DOE Symposium on Improved Oil Recovery*, number SPE 113496, Tulsa OK, USA, 2008. Society of Petroleum Engineers.

[15] R. Juanes, E. J. Spiteri, F. M. Orr Jr., and M. J. Blunt. Impact of relative permeability hysteresis on geological CO_2 storage. *Water Resources Research*, 42(W12418), 2006.

[16] H. B. Keller. *Numerical methods for two-point boundary-value problems*. Dover, New York, 1992.

[17] I. N. Kochina, N. N. Mikhailov, and M. V. Filinov. Groundwater mound damping. *International Journal of Engineering Science*, 21(4):413–421, 1983.

[18] K. S. Lackner. Climate change: a guide to CO_2 sequestration. *Science*, 300(5626):1677–1678, 2003.

[19] R. Lenormand, C. Zarcone, and A. Sarr. Mechanisms of the displacement of one fluid by another in a network of capillary ducts. *Journal of Fluid Mechanics*, 135:337–353, 1983.

[20] S. Lyle, H. E. Huppert, M. Hallworth, M. Bickle, and A. Chadwick. Axisymmetric gravity currents in a porous medium. *Journal of Fluid Mechanics*, 543:293–302, 2005.

[21] M. Muskat. The flow of fluids through porous media. *Journal of Applied Physics*, 8(4):274–282, 1937.

[22] M. Muskat and M. W. Meres. The flow of heterogeneous fluids through porous media. *Physics*, 7(9):346–363, 1936.

[23] J. M. Nordbotten, M. A. Ceila, and S. Bachu. Injection and storage of CO_2 in deep saline aquifers: analytical solution for CO_2 plume evolution during injection. *Transport in Porous Media*, 58(3):339–360, 2005.

[24] J. M. Nordbotten and M. A. Celia. Similarity solutions for fluid injection into confined aquifers. *Journal of Fluid Mechanics*, 561:307–327, 2006.

[25] F. M. Orr. Storage of carbon dioxide in geological formations. *Journal of Petroleum Technology*, (9):90–97, 2004.

[26] D. Pritchard. Gravity currents over fractured substrates in a porous medium. *Journal of Fluid Mechanics*, 584:415–431, 2007.

[27] D. P. Schrag. Preparing to capture carbon. *Science*, 315(5813):812–813, 2007.

[28] R. D. Wyckoff and H. G. Botset. The flow of gas-liquid mixtures through unconsolidated sands. *Physics*, 7(9):325–345, 1936.

[29] Y. C. Yortsos. A theoretical analysis of vertical flow equilibrium. In *SPE Annual Technical Conference and Exhibition*, number 22612-MS, Dallas, TX, 1991. Society of Petroleum Engineers.

[30] Y. C. Yortsos. A theoretical analysis of vertical flow equilibrium. *Transport in Porous Media*, 18(2):107–129, 1995.